CRACK DETECTION BY ULTRASONIC METHODS: THEORY AND EXPERIMENT

J. D. Achenbach* and L. Adler**

*Department of Civil Engineering, Northwestern University, Evanston, IL 60201, USA

**Department of Physics, University of Tennessee, Knoxville, TN 37916, USA

ABSTRACT

In this paper analytical solutions to the diffraction of elastic waves by penny-shaped and elliptical cracks in metals have been compared with experimental observations. The analytical results are for waves in the high-frequency domain. In the experimental work a digitized spectrum analysis system was used to measure the frequency components of the waves scattered by a crack in a circular disk of titanium alloy, which was immersed in a water bath. Analytical and experimental results show very satisfactory agreement. The theoretically predicted modulation of the amplitude spectrum provides a simple formula for the inverse problem. Application of this formula to the experimental measurements determines the crack size with excellent accuracy.

KEYWORDS

Non-destructive testing; ultrasonic waves; scattering by cracks; high-frequency analysis; digitized spectrum analysis; penny-shaped cracks; titanium specimens.

INTRODUCTION

One of the most useful methods in quantitative non-destructive evaluation (QNDE) of structural elements is based on the scattering of elastic (ultrasonic) waves by flaws in solids. Two general approaches to ultrasonic flaw detection can be taken. The imaging approach seeks to process the scattered field in such a manner that a visual outline of the object is produced on a display. The scattered-field approach attempts to infer geometrical characteristics of a flaw from either the angular dependence of its far-field scattering amplitude at fixed frequency, or from the frequency dependence of its far-field scattering amplitude at fixed angle. This paper is concerned with analytical and experimental investigations for the scattered-field approach to crack-like flaws.

Transient pulses can be written as superpositions of time-harmonic signals. For short pulses the frequency spectra of the scattered signals are centered in the high-frequency (short wavelength) range. When the probing wavelength is short, there are many interference processes whose characteristic forms can provide the basis for an inversion procedure. Particularly the first arriving signals, which are related to the longitudinal waves in the solid have a very simple structure.

The experimental work was carried out by the use of a digitized ultrasonic spectrum analysis system. The experimental setups included instrumentation to gate-out and spectrum analyze the signal scattered by the crack. The raw scattering data was corrected for transducer transfer functions and other characteristics of the system, which were obtained on the basis of appropriate calibrations. After processing, the amplitudes as functions of the frequency, were compared with analytical results.

Ray Theory

At high frequencies the diffraction of elastic waves by cracks can be analyzed conveniently on the basis of elastodynamic ray theory. For time-harmonic wave motion, ray theory provides a method to trace the amplitude of a disturbance as it propagates along a ray. In a homogeneous, isotropic, linearly elastic solid the rays are straight lines, which are normal to the wavefronts. An unbounded solid can support rays of longitudinal and transverse wave motion. These rays are denoted as L-rays and T-rays, respectively. The free surface of a solid can, in addition, support rays of surface-wave motion, which are denoted as R-rays.

In analogy with geometrical optics, the simplest theory for diffraction of elastic waves by cracks may be called geometrical elastodynamics (GE). In GE a crack acts as a screen, which creates a shadow zone of no motion, and zones of reflected waves. The displacement field according to GE, which is denoted by $\underset{\sim}{u}^g$, is of the same order of magnitude as the incident field.

The geometrical theory of diffraction (GTD) provides a first correction to GE. This correction is valid for $\omega a/c_L >> 1$, and at points where $S/a > 1$. Here ω is the circular frequency, a is a length dimension of the crack, c_L is the velocity of longitudinal waves, and S is the distance from a crack edge. The correction provided by GTD is of order $(\omega a/c_L)^{-1/2}$.

Basic to GTD is the result that the incidence of a body-wave ray on the edge of a crack gives rise to two cones of diffracted body-wave rays and two R-rays (one on each crack face). The surfaces of the inner and outer cones of body-wave rays consist of L-rays and T-rays, respectively. When an R-ray intersects the edge of a crack, a ray of reflected surface wave motion is generated, as well as cones of diffracted body-wave rays. The analytical details for the computation of the fields on the diffracted and reflected rays have been worked out by Achenbach, Gautesen and McMaken, (1977, 1978a).

With GE and GTD the total displacement field is of the form

$$\underset{\sim}{u}^t = \underset{\sim}{u}^g + \underset{\sim}{u}^d \qquad (1)$$

This result is not valid at the boundaries of the shadow zone and the zone(s) of reflected waves. In a further refinement which is called uniform asymptotic theory (UAT), the fields at these boundaries are corrected. For diffraction by a slit details can be found in a paper by Achenbach, Gautesen and McMaken (1978b).

For incident waves with curved wavefronts and for curved diffracting edges, the cones of diffracted rays have envelopes, at which the rays coalesce and the fields become singular. The envelopes are called caustics, and GTD breaks down at caustics.

Within the context of the GTD theory of Achenbach et al (1977, 1978a,b), the diffracted field at a point of observation Q is comprised of contributions corresponding to "primary" diffracted body-wave rays, which are directly generated by incident body-wave rays, and contributions corresponding to "secondary"

diffracted body-wave rays. The latter are generated by rays travelling via the crack faces.

Numerical results obtained by GTD have been compared with exact results for normal incidence on slits and penny-shaped cracks. Very good agreement was generally observed, see Achenbach et al (1978b,c).

Diffracted L-rays in the solid. For normal incidence of a plane longitudinal wave, the displacement vectors on the diffracted L-rays in the solid are

$$\underset{\sim}{u}_L = \exp(i\omega S/c_L)\,(\omega S/c_L)^{-1/2}\,(1+S/C)^{-1/2} D_L^L(\theta)\,\underset{\sim}{i}_L U_o \qquad (2)$$

Here S is the distance along a diffracted ray from the point of diffraction to the point of observation, c_L is the velocity of longitudinal waves, and θ is the angle of the diffracted ray with the diffracting surface. The geometrical quantities are indicated in Fig. 1. The amplitude U_o defines the incident wave in the plane of the crack, and C is the distance to the caustic. For a penny-shaped crack under normal incidence the caustic is the normal through the center of the crack, i.e., $C = -a/\cos\theta$, where a is the radius of the penny-shaped crack. The vector $\underset{\sim}{i}_L$, which defines the direction of the displacement, is radial from the point of diffraction. The dimensionless diffraction coefficent is denoted by $D_L^L(\theta)$.

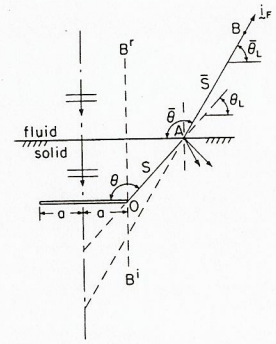

Fig. 1. Diffracted ray from a crack tip in an immersed specimen.

Transmission across the solid-fluid interface. The incidence of an L-ray from the solid side on a solid-fluid interface generates an L-ray of transmitted motion in the fluid and reflected L- and T-rays in the solid. The geometry for a single ray is shown in Fig. 1. Along the L-ray in the fluid the field is of the general form

$$\underset{\sim}{u}_L = \exp(i\omega\bar{S}/c_F)(1+\bar{S}/\bar{C})^{-1/2}\,(1+\bar{S}/\bar{E})^{-1/2}\,T(\theta_L)\,U_A\,\underset{\sim}{i}_F \qquad (3)$$

Here c_F is the velocity of longitudinal waves in the fluid, $\bar{S}$ is the distance from the point of transmission A to the point of observation B, U_A defines the incident field at A, and the unit vector $\underset{\sim}{i}_F$ defines both the direction of the transmitted ray and the displacement

direction on that ray, see Fig. 1. The terms $(1 + \overline{S}/\overline{C})^{-1/2}$ and $(1 + \overline{S}/\overline{E})^{-1/2}$ follow from considerations of energy conservation in a bundle of rays in the fluid. It remains to determine $\overline{C}$, $\overline{E}$, $\overline{\Theta}_L$ as well as the transmission coefficient $T(\Theta_L)$ as functions of the angle of incidence θ_L. Note that in the present geometry $\Theta_L = \pi - \Theta$ and $\overline{\Theta}_L = \pi - \overline{\Theta}_L$. The derivation of $\overline{C}$, $\overline{E}$, $\overline{\Theta}_L$, and $T(\Theta_L)$ is carried out in a paper by Achenbach, et al (1979b). The transmission coefficient, $T(\Theta_L)$, is determined from specific interface conditions. We assume, as is usually done, that the normal displacement and the normal stress component are continuous at the fluid-solid interface, while the shear stress in the solid vanishes at the interface.

The COD-RT approach

In this section a hybrid theory is discussed in which the crack-opening displacement (COD) is computed on the basis of elastodynamic ray theory, and the diffracted field is subsequently obtained by the use of a representation theorem (RT). The advantage of this approach is that the trouble with ray theory at shadow boundaries and boundaries of zones of specular reflection is eliminated, and caustics only need to be dealt with on the faces of the crack.

The field generated by scattering of incident waves by an obstacle with surface S can be expressed in terms of a representation integral over S. For a stress-free crack with plane faces A^+ and A^- the representation integral can be simplified. If the total field is written as $\underset{\sim}{u}^t = \underset{\sim}{u}^{in} + \underset{\sim}{u}^{sc}$, where $\underset{\sim}{u}^{in}$ is the incident field and $\underset{\sim}{u}^{sc}$ is the scattered field, then at an arbitrary field $\underset{\sim}{x}$ the latter can be expressed in the form

$$u_j^{sc}(\underset{\sim}{x}) = \int_{A^+} \tau_{i3;j}^{G}(\underset{\sim}{x}-\underset{\sim}{X})\, \Delta u_i^{sc}(\underset{\sim}{X})\, dA(\underset{\sim}{X}) \tag{4}$$

Here the crack is in the X_1X_2-plane and the positive X_3-axis is pointing into the material at the A^+ crack-face. Also $\Delta u_i(X)$ is the crack-opening displacement defined by

$$\Delta u_i^{sc}(\underset{\sim}{X}) = (u_i^{sc})^{A^+} - (u_i^{sc})^{A^-}, \tag{5}$$

and

$$\tau_{i3;j}^{G} = \text{tensor of rank three}, \tag{6}$$

which represents the stress-components at $X_3 = 0$ due to a unit load in the X_j direction at the point defined by $\underset{\sim}{X} = \underset{\sim}{x}$.

Equation (4) can be integrated numerically. A further simplification is, however, achieved if it is assumed that the origin 0 is close to the crack while the source S and the observation point Q are far away, see Fig. 2. The expression for $\tau_{ij;m}^{G}$ then simplifies considerably. An explicit expression can be found in Achenbach et al (1979a).

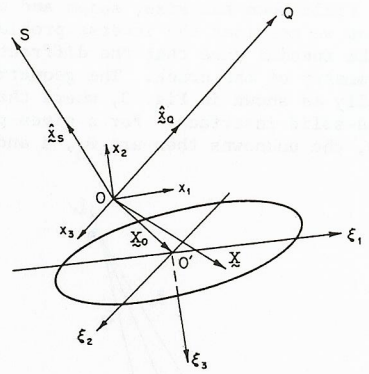

Fig.2. Flat crack with source point S and point of observation Q.

Physical elastodynamics

In the physical elastodynamics approximation only the leading contributions arising from the incident wave and the specularly reflected body waves are included in Δu^{sc}. Thus, the effect of the crack edge on the displacement discontinuity of the crack faces is neglected. This is thought to be acceptable if the wavelength is sufficiently smaller than the cross-sectional dimensions of the crack.

On the faces of the crack the spherical wave emitted at S is locally approximated by a plane wave:

$$\underset{\sim}{u}^{in} = - A\, \hat{\underset{\sim}{x}}_S\, G_L(x_S) \exp(-ik_L \hat{\underset{\sim}{x}}_S \cdot \underset{\sim}{X}) \quad , \quad x_S >> X \tag{7}$$

where

$$G_L(x_S) = (1/4\pi x_S) \exp(ik_L x_S) \tag{8}$$

$$k_L = \omega/c_L \quad , \quad c_L^2 = (\lambda+2\mu)/\rho \tag{9}$$

and $\hat{\underset{\sim}{x}}_S = \underset{\sim}{x}_S/x_S$, $x_S = |\underset{\sim}{x}_S|$, $X = |\underset{\sim}{X}|$. By using some well known results for reflection of plane waves we then find

$$\Delta \underset{\sim}{u}^{sc} \sim \underset{\sim}{u}^{GE} = A\, \Delta \underset{\sim}{U}\, G_L(x_S) \exp(-ik_L \hat{\underset{\sim}{x}}_S \cdot \underset{\sim}{X}) \tag{10}$$

where

$$\underset{\sim}{U}(\hat{\underset{\sim}{x}}_S) = - \underset{\sim}{p} - R_L \underset{\sim}{p}_L - R_T \underset{\sim}{d}_T \tag{11}$$

Here $\underset{\sim}{p}$, $\underset{\sim}{p}_L$ and $\underset{\sim}{d}_T$ are unit vectors defining the displacement directions of the incident and reflected waves, and R_L and R_T are the reflection coefficients.

For a crack of elliptical shape the resulting expression for the scattered field which follows by substitution of (10) in (4), can be evaluated to yield an ordinary Bessel function of order one (Adler and Achenbach, 1980).

The Inverse Problem

Previous sections have been concerned with the direct problem, that is the com-

putation of the scattered field when the size, shape and orientation of the crack are known. In this section we consider the inverse problem for plane waves incident on cracks, for the special case that the diffracted field is symmetric relative to a plane of symmetry of the crack. The geometry in the plane of symmetry is then essentially as shown in Fig. 3, where the crack is under an angle Θ_o with the fluid-solid interface. For a given point of observation, say the point B in Fig. 3, the unknowns then are Θ_o, a and b.

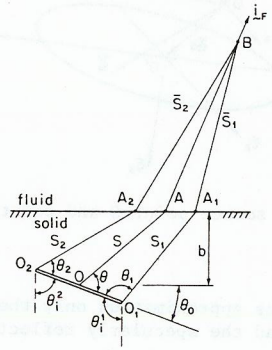

Fig. 3. Geometry in the plane of symmetry of a penny-shaped crack.

The frequency spectrum of longitudinal signals contains a considerable amount of information on the crack. To obtain the size and orientation of the crack, experimental information can be used both for direct comparison (particularly of the amplitude modulation) with analytical results and as an input to an inversion integral. These interpretations of experimental results, which both lean heavily on theoretical results, will now be discussed.

Direct interpretation of amplitude modulations. The interference patterns for the first arriving longitudinal waves in the fluid are generated by phase differences and amplitude differences on the direct rays from the two crack tips. Adding the primary diffracted longitudinal fields from the points O_1 and O_2, we obtain after introducing some far-field simplifications

$$\underset{\sim}{u}_L \sim F(\Theta,\Theta_o)\, \exp[i\omega(S/c_L + \bar{S}/c_F) + i\pi/4]\, U_o\, \underset{\sim}{i}_F \qquad (12)$$

where

$$F(\Theta,\Theta_o) = H_1 \exp[-i(\omega a/c_L)(\cos\Theta - \sin\Theta_o)] + H_2 \exp[i(\omega a/c_L)(\cos\Theta - \sin\Theta_o)] \qquad (13)$$

The terms H_1 and H_2 do not depend on the frequency. Explicit expressions for H_1 and H_2 are given by Achenbach et al (1979b).

Of particular interest is the absolute magnitude of F,

$$|F| = \{H_1^2 + H_2^2 + 2H_1H_2 \sin[2(\omega a/c_L)(\cos\Theta - \sin\Theta_o)]\}^{1/2} \qquad (14)$$

This result implies that the amplitude of the primary diffracted field is modulated with respect to ω/c_L with period

$$P = \frac{\pi}{a|\cos\Theta - \sin\Theta_o|} \qquad (15)$$

Application of inversion integrals. Inversion integrals for crack-scattering data have been discussed in some detail by Achenbach et al (1979a).

EXPERIMENTS

Experimental System

The details of the ultrasonic data acquisition and processing system have been discussed by Adler and Achenbach (1979b, 1980). A SCR pulser produces a fast rise-time high voltage (162 volts) negative spike with an exponential return to zero. This wide band electrical pulse excites an untuned, highly damped ceramic transducer with center frequency of 10 Mhz. The ultrasonic pulse (pulse length ~ 1 μsec) which is produced contains a broad band of frequencies. Ultrasound scattered by the target is received by either [1] the transmitting transducer [pulse-echo] or [2] a receiving [identical] transducer [pitch-catch]. The electrical pulse produced by this receiving transducer is amplified by a wide bandwidth gain stage. A stepless gate is used to select a portion of the received signal for further analysis. Signals falling outside the gated regions are highly attenuated. An oscilloscope displays both the entire receiver output and the section of waveform passed by the gate.

The frequency content of the gated waveform is produced by an analog spectrum analyzer. The gated pulse may also be captured and stored through use of the digital acquisition system. A transient recorder samples the ultrasonic signal at 100 MHz, and stores the amplitude at discrete times in its digital memory. The minicomputer controls the acquisition of the ultrasonic pulse and then transfers the digitally represented signal from the recorder to the minicomputer memory. The signal may also be permanently stored by recording it onto magnetic tape. Processing of the ultrasonic signal [Fast Fourier Transform, correlation and deconvolution] is performed on the minicomputer. An electrostatic plotter provides a visual display of pertinent information. For the Fourier Transform both amplitude and phase spectra can be calculated. In this experiment the amplitude spectra are used only. The digital amplitude spectra is monitored by the analog spectra [i.e., the spectrum offered by the spectrum analyzer].

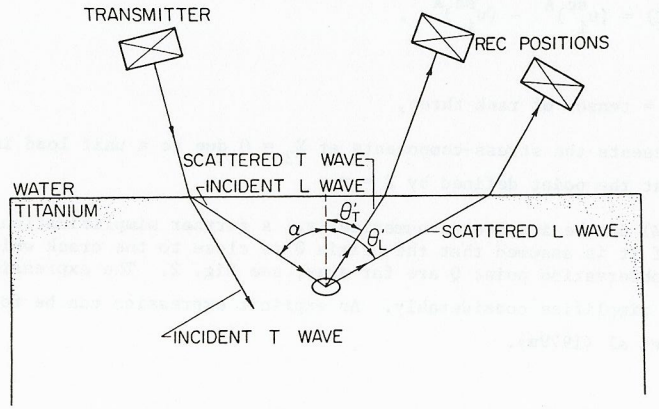

Fig. 4. Experimental configuration.

Experimental Technique

The configuration for the experimental work is shown in Fig. 4. The sample containing a defect with flat faces is immersed in water. The transmitter launches a longitudinal wave to the liquid-solid interface at some angle. For nonnormal incidence both L and T waves are produced in the metal. The cavity can be insonified either by the L wave or by the T wave with incident angle α. At the cavity the waves are scattered and mode converted. The scattered waves are received and analyzed separately due to their separation in arrival time.

A specially designed goniometer is used to mount the transmitter and the receiver. The position of both transmitter and receiver in polar angle can be changed separately. A special feature of the goniometer is its flexibility of keeping the polar angle fixed and varying the azimuthal angle. This latter feature is especially important for noncircular cracks because of the asymmetry in the scattered field along the different directions.

Data Correction

In order to analyze the experimental results based on the analytical prediction, the effect of the transducers and the crack had to be separated. In a linear time variant system this is done in the frequency domain by dividing the frequency response from a system by the so-called transfer function. In this problem the spectrum of the transmitted signal through the material [without the crack] is considered the transfer function.

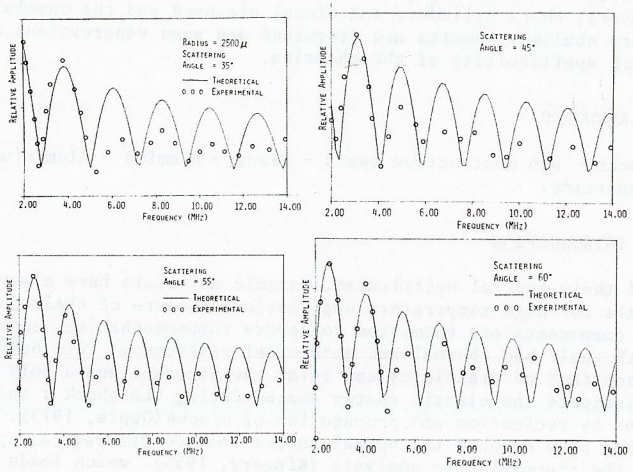

Fig. 5. Amplitude spectra of scattered longitudinal waves

COMPARISON WITH EXPERIMENTAL DATA

For normal incidence of a longitudinal wave on a penny-shaped crack, the field corresponding to scattered longitudinal waves at the point of observation in the water has been computed by adding the two contributions according to Eq.(3) emanating from the two crack tips. Analytical and experimental results are compared in Fig. 5. The analytical amplitude spectra are plotted by the solid lines while the experimentally obtained amplitude spectra are shown by the circles. The frequency varies from 2 MHz to about 14 MHz. The scattered angles ($\theta_L' = \pi/2 - \theta_L$) are 35^o, 45^o, 55^o, and 60^o, respectively, in the solid. The amplitudes of the first cycles agree well for all angles. At higher frequencies (above 6 MHz) the experimental results are lower than the predicted theory. One possible explanation is the effect of attenuation which is not accounted for in the theory. In all cases the positions of maxima and minima of the spectra agree, however, very well between theory and experiment. The positions of these maxima are significant for the inversion procedure.

For normal incidence of a longitudinal wave on an elliptical crack of semi major and semi minor axes of 2500μ and 1250μ, respectively, the scattered field according to the physical elastodynamics theory is compared with experimental results in Fig. 6. Considering that the theory is very simple the results can be considered very satisfactory. The experimental results decay faster with frequency than the theoretical ones, but the spacing of the peaks shows very good agreement. It is noted that the inclusion of some damping in the theory improves the agreement.

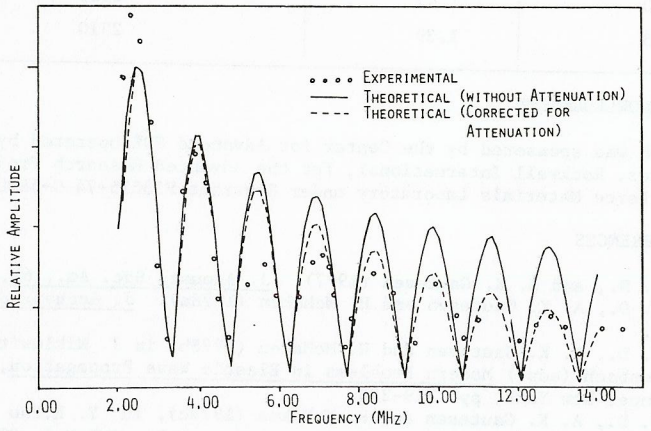

Fig. 6. Comparison of theory and experiment for a crack of elliptical shape, for normal incidence and a scattering angle $\theta_L' = 60^o$ in the plane of the major axis.

Finally we show an experimental verification of Eq.(15). In the experimental results shown in Fig. 5 the plane of the crack is parallel with the fluid-solid interface, and hence $\theta_o = 0$. From each amplitude spectrum in Fig. 5 we can then obtain the radius of the crack. The radius a of the crack follows from Eq.(15) as

$$a = \frac{c_L}{2 \sin(\theta_L') \Delta(f_{max})} \qquad (16)$$

where $\theta_L' = \frac{\pi}{2} - \theta$ and $\Delta(f_{max})$ is the average frequency spacing between two consecutive maxima.

In Table I the result of the size determination from the spectral components of the diffracted wave is given. The agreement between actual crack size (a = 2500μ) and the predicted value is excellent. The largest deviation is 3.7 % .

TABLE 1 Computation of the Crack Radius from Eq.(16)

Scattering Angle θ_L'	$\Delta(f_{max})$	Computed Radius of the Crack in μ
35°	2.18	2530
40	1.87	2630
45	1.83	2450
50	1.68	2460
55	1.60	2410
60	1.47	2500
65	1.39	2510

ACKNOWLEDGEMENT

This research was sponsored by the Center for Advanced NDE operated by the Science Center, Rockwell International, for the Advanced Research Projects Agency and the Air Force Materials Laboratory under Contract F33615-74-C-5180.

REFERENCES

Achenbach, J. D., and A. K. Gautesen (1977). J. Acoust. Soc. Am., 61, 413-421.

Achenbach, J. D., A. K. Gautesen and H. McMaken (1978a). J. Acoust. Soc. Am., 63, 1824-1831.

Achenbach, J. D., A. K. Gautesen and H. McMaken (1978b) in J. Miklowitz and J. D. Achenbach (eds.) Modern Problems in Elastic Wave Propagation, Wiley Interscience, New York, pp. 219-238.

Achenbach, J. D., A. K. Gautesen and H. McMaken (1978c), in Y. H.Pao (Ed.) Elastic Waves and Non-Destructive Testing of Materials, AMD-Vol. 29, American Society of Mechanical Engineers, pp. 33-52.

Achenbach, J. D., K. Viswanathan, and A. Norris (1979a). Wave Motion, 1, 299-316.

Achenbach, J. D., L. Adler, D. Kent Lewis, and H. McMaken (1979b). J. Acoust. Soc. Am., 66, 1848-1856.

Adler, L. and J. D. Achenbach (1980). J. of Nondest. Ev., in press.